Showcasing research from Professor Haresh Manyar's laboratory, School of Chemistry and Chemical Engineering, Queen's University Belfast, UK.

Structure sensitivity of Cu supported on manganese oxide catalysts in levulinic acid hydrogenation

Better and more efficient Copper catalysts were prepared by making copper nanoparticles smaller and smaller for structure-sensitive reaction of levulinic acid hydrogenation to gamma-valerolactone.

As featured in:

See Haresh Manyar *et al.*,
Catal. Sci. Technol., 2024, **14**, 840.

ROYAL SOCIETY OF CHEMISTRY

rsc.li/catalysis

PAPER

Structure sensitivity of Cu supported on manganese oxide catalysts in levulinic acid hydrogenation†

Nayan Jyoti Mazumdar, [iD] [a] Praveen Kumar,[b] Miryam Arredondo-Arechavala,[b] Nancy Artioli[ac] and Haresh Manyar [iD] *[a]

Different synthesis methods were used to prepare a series of size-controlled copper nanoparticles supported on manganese oxide octahedral molecular sieve (OMS-2) catalysts. All Cu/OMS-2 catalysts, with average Cu nanoparticle sizes prepared in the range of 2–22 nm, were thoroughly characterised using X-ray diffraction (XRD), N_2 sorption, H_2 temperature programmed reduction (TPR), transmission electron microscopy (TEM), and ICP-OES elemental analyses. The catalytic activity of the size-controlled Cu/OMS-2 catalysts was investigated in liquid phase hydrogenation of levulinic acid as a model reaction to evaluate the nanoparticle size dependance and structure–activity relationship. The catalytic activity studies showed that the catalyst performance depends greatly on the catalyst preparation methodology and Cu nanoparticle size. Complete conversion of levulinic acid with a high γ-valerolactone yield, >99%, was observed using Cu/OMS-2 catalysts prepared by the precipitation–deposition (Cu nanoparticle size 2–3 nm) method. In comparison to wet-impregnated catalysts (Cu particle size 20–22 nm), the improved performance of precipitation–deposition catalysts was mainly attributed to the well-distributed, smaller Cu nanoparticles. The influence of Cu nanoparticle size is correlated with the turnover frequency (TOF, h^{-1}) for levulinic acid conversion, indicating the structure sensitivity of the levulinic acid hydrogenation reaction.

1. Introduction

Recent advances in nanomaterial synthesis allow us to have better control over the size and shape of metal nanoparticles leading to unique and superior physico-chemical properties. This opens new possibilities in catalysis to design more efficient and improved supported nanoparticle catalysts by controlling the size, shape, and composition of metal nanoparticles. Traditionally, heterogeneous catalysis by metals involves the impregnation of precursor salts on high surface area supports to synthesize highly dispersed metal nanoparticles. This strategy yields thermodynamically stable quasi-spherical metal nanoparticles. The distribution of active sites on metal nanoparticles is size and shape dependent, which determines the catalytic activity of nanoparticles in structure-sensitive reactions affecting the reaction rates and product distribution.

[a] *School of Chemistry and Chemical Engineering, Queen's University Belfast, David-Keir Building, Stranmillis Road, Belfast, BT9 5AG, UK.*
E-mail: h.manyar@qub.ac.uk
[b] *School of Mathematics and Physics, Belfast, BT7 1NN, UK*
[c] *Department of Civil, Environmental, Architectural Engineering and Mathematics, University of Brescia, Via Branze, 43, 25123 Brescia, Italy*
† Electronic supplementary information (ESI) available. See DOI: https://doi.org/10.1039/d3cy01064c

Levulinic acid (LA) hydrogenation to γ-valerolactone (GVL) using heterogeneous catalysts with supported noble metals Ru, Pd, Pt, Ni, Rh, Ir, Au *etc.* has been extensively investigated under both gas phase and liquid phase conditions.[1] Industrial-scale implementation and upscaling face considerable challenges due to the high costs and limited availability of noble metals. Non-noble metal heterogeneous supported catalysts are cheap and easily available, which is also significant in terms of cost reduction. The catalytic activity of earth-abundant metals, such as Cu, is typically lower than that of precious metals.[2] Surface chemistry techniques have indicated that the structure and size of metal particles considerably affect the catalytic properties, while studies on sub-nanometer metal clusters in heterogeneous catalysis have revealed distinct size-dependent trends.[3,4] Step-edge surface sites has been explored to gain more insights into their capability in reducing energy barriers during the adsorption of reactants and products in chemical reactions in order to improve the catalytic activity.[5] Metal nanoparticles (NPs) with size of less than 10 nm modify the surface in contact with the adsorption sites and alter the surface structure.[6] In transition metal nanoparticles, the particles with size >10 nm have their surface determined by the termination of the bulk structure, while smaller particles <10 nm show interactions between surface energies and bulk

840 | *Catal. Sci. Technol.*, 2024, **14**, 840–849

This journal is © The Royal Society of Chemistry 2024

structure energies, resulting in the formation of metal clusters and various particle shapes and sizes.[6] These factors significantly affect the chemical activity of particles smaller than 10 nm. Metal clusters can behave like molecules, where their reactivity can be controlled by their orbital structure, or they can behave like bulk structures, which in turn impacts the catalytic activity in structure-sensitive reactions. Furthermore, metal nanoparticles with a size range of 2–10 nm has been found to have a significant effect on the catalytic activity and product selectivity for hydrogenation reactions and dissociation reactions.[7–12] In LA hydrogenation to GVL, precious metal catalysts like ruthenium (Ru) supported on titania (TiO_2), ZSM-5, and as nanoparticles (NPs) have shown excellent activity under varying reaction conditions (70–200 °C, 1–40 bar H_2), achieving high LA conversion (>99%) and GVL yield (>96%).[13–15] However, these metals also suffer from inherent disadvantages, like scarce availability, high cost, and toxicity. In this regard, the use of more sustainable metals is necessary, and the catalysts based on earth-abundant transition metals, which are low in cost and easily available have proven as attractive alternatives. Copper is one such metal, which is easily available and has been extensively studied in hydrogenations.

Due to the increasing global population and technological developments, our society is facing a rise in overall energy consumption. Projections show that investments in energy for the year 2023 are anticipated to reach approximately USD 2.8 trillion.[16] In 2022, there was a 0.9% increase in global energy-related CO_2 emissions, reaching a new record of more than 36.8 billion metric tons of CO_2.[17] Countries are applying various protocols to reduce CO_2 emissions and combat global warming by decreasing utilisation of fossil fuels and shifting to renewable, and sustainable energy alternatives.[18] Biomass-derived platform chemicals, such as LA, have been identified as an important intermediate platform chemical which can be further upgraded to produce biofuels and biofuel additives.[19] LA can be converted to produce value-added chemicals such as γ-valerolactone, 5-hydroxymethylfurfural, levulinate esters and 2-methyltetrahydrofuran.[20] As proposed in Scheme 1, LA undergoes dehydration leading to the

formation of α-angelica lactone (α-AL). α-AL is further hydrogenated to produce GVL. GVL is a promising alternative to bioethanol due to its lower vapor pressure, high boiling point, and energy density and can be utilised as solvents, fuel additives, and even in the production of nylon intermediates.[21] Furthermore, GVL can be upgraded to jet-fuel blends *via* formation of C_4 alkenes.[22,23]

Rode *et al.* demonstrated Cu supported on Al_2O_3, and ZrO_2 showed good selectivity towards GVL.[24] Zhang and co-workers investigated Ag–Cu/Al_2O_3 to suppress leaching of Cu and improve re-usability of the catalyst.[25] Despite many studies over Cu-based catalysts, there is still a gap in understanding the active species of Cu participating in the reaction. Several research groups have suggested an interaction between Cu species, which participate as Cu^0 and Cu^+ with mixed-metal oxide support to influence the catalytic activity.[26–30] There is still a need to investigate the role of Cu-support effects and the effect of Cu particle size to enhance the hydrogenation activity, for a rational design of an improved catalyst. Recently, we have synthesised and evaluated a series of Cu supported on manganese oxide octahedral molecular sieve (OMS-2) catalysts and showed that 20 wt% Cu/OMS-2 (average Cu size 27 nm) exhibited good activity for LA hydrogenation.[31] Other studies have also demonstrated that an average size of 15 nm for NPs are attributed to high dispersion of Cu on its support, which results in the conversion of LA to GVL with high yield.[32] In the literature, LA hydrogenation is known for its structure sensitivity and the influence of metal nanoparticle size on catalytic activity. Ruppert *et al.* studied Ru/TiO_2 catalysts and found that the optimal Ru particle size for LA hydrogenation was within the range of 3–4 nm.[33] Similarly, Berg *et al.* investigated the impact of copper particle size within the range where surface structure changes occur, specifically below 10 nm, in methanol synthesis reaction.[7] Decreasing the size of copper particles enhanced the dispersion, leading to higher catalytic activity. Recently our group has demonstrated high activity and selectivity using manganese oxide OMS-2 based catalysts in a range of hydrogenation, oxidation, and decomposition reactions.[34–46] We have also
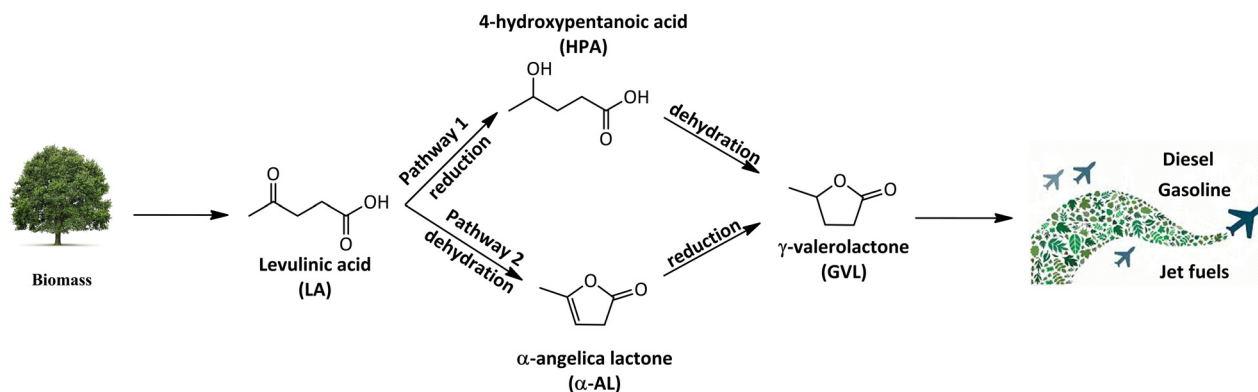
Scheme 1 Reaction pathways for the synthesis of γ-valerolactone and green aviation fuels from levulinic acid.

This journal is © The Royal Society of Chemistry 2024

Catal. Sci. Technol., 2024, **14**, 840–849 | **841**

shown the utilisation of Pt doped OMS-2 as selective hydrogenation catalysts for cinnamaldehyde reduction, with high selectivities to cinnamyl alcohol.[47,48] Pt/OMS-2 was shown as an efficient and selective hydrogenation catalyst, further enhanced with Pt-doping, which was attributed to water assisted H_2-dissociation.[49]

In this study, we have investigated the catalytic activity of supported Cu nanoparticle catalysts for the hydrogenation of LA to GVL. We have established the synthesis protocols for size control of Cu nanoparticles in the range of 2 to 27 nm. We further evaluated the catalytic activity of the prepared Cu/OMS-2 catalysts in LA hydrogenation, and correlated the turnover frequencies with Cu nanoparticle sizes. For development of more sustainable processes, using earth abundant metal catalysts such as Cu instead of precious noble metal catalysts would go a long way.

2. Experimental section

2.1 Materials

Levulinic acid ($C_5H_8O_3$, 98%), copper nitrate hemipentahydrate ($Cu(NO_3)_2 \cdot 2.5H_2O$, 98%), copper(II) oxide (CuO, ≥99.0%) and 1,4-dioxane ($C_4H_8O_2$, 99%) were purchased from Alfa Aesar. γ-Valerolactone ($C_5H_8O_2$, 99%), α-angelica lactone ($C_5H_6O_2$, 98%), tetrahydrofuran (($CH_2)_4O$, 98%) and maleic acid ($C_4H_4O_4$, 98%) were purchased from Sigma Aldrich. Potassium permanganate ($KMnO_4$, 98%) and ammonium bicarbonate (NH_4HCO_3, 99%) were procured from Honeywell Fluka. All chemicals were used without any further purification.

2.2 Catalyst preparation

2.2.1 Synthesis of manganese oxide octahedral molecular sieve (OMS-2).
OMS-2 was synthesised using the sol–gel method, as reported from our previous work.[31] In summary, a measured amount of $KMnO_4$ was added in deionised water and stirred for 1 h. Maleic acid was slowly added to this solution in a molar ratio of 3 : 1, and the solution was further stirred for 3 h at room temperature. A dark brown gel was formed on the top layer which was allowed to settle and then decanted off. Deionised water was added, and the solution was stirred again for 10 min and the process was repeated for three times. The resultant mixture was vacuum filtered to separate excess water and dried overnight in the oven at 120 °C. The dried OMS-2 was calcined at 450 °C for 3 h in the presence of air.

2.2.2 Synthesis of Cu/OMS-2 catalysts by wet-impregnation.
A series of varying wt% of Cu supported on OMS-2 was prepared using the wet-impregnation method and denoted with (Wet-Imp) in the name. First, a required amount of $Cu(NO_3)_2 \cdot 2.5H_2O$ was dissolved in water. After the solution was stirred for 25 min, OMS-2 was slowly added to the solution and the mixture was stirred at 450 rpm under room temperature for 3 h. The temperature was set to 70 °C to slowly evaporate the water and after 3 h the slurry was kept inside an oven at 110 °C for overnight drying. It was then calcined at 550 °C for 6 h.

2.2.3 Synthesis of Cu/OMS-2 catalysts by precipitation–deposition.
To observe the effect of preparation methods, varying wt% of Cu supported on OMS-2 were also to synthesised by precipitation–deposition method and denoted with (Pre-Dep) in the name. In this method, ammonium bicarbonate (1 M) solution was used as a precipitant with the aim to decrease the Cu particle size and increase the copper dispersion on the support. In a typical synthesis, a measured amount of $Cu(NO_3)_2 \cdot 2.5H_2O$ was dissolved in water in a three neck round bottle flask under magnetic stirring for 25 min. OMS-2 was slowly added to the solution and continuously stirred for 3 h. NH_4HCO_3 (1 M) was added dropwise to the resulting solution for precipitation, until the pH of the solution reached 9. Once a pH of 9 was reached the solution was aged for 24 h. After the aging process was complete, the mixture was refluxed at a temperature of 85 °C for 5 h. The catalyst was then recovered by vacuum filtration and oven-dried overnight at 110 °C. It was then calcined under air at 450 °C, 10 °C min^{-1} for 3 h.

2.3 Catalyst to characterisation

Powder X-ray diffraction (XRD) measurements were performed with CuK α-radiation (1.5405 Å) on a PANalytical X'PERT PRO MPD diffractometer, equipped with a nickel filter, and operated at 40 kV and 40 mA. The scattered X-ray intensities were measured between 5 to 80° (2θ) with a counting time of 0.5 s. Scherer's equation was applied to determine the mean size of Cu NPs.

$$d = \frac{0.9\lambda}{\beta \cos\theta}$$

where d is the mean diameter of Cu NPs (nm), λ is the wavelength of the X-ray radiation source (nm), β is the full width at half maximum (FWHM, radians) of the peak at the given diffraction angle, 2θ.

The specific surface area, pore volume and average pore diameter were determined by N_2 adsorption–desorption isotherms at 77 K using a Micromeritics ASAP 2020 instrument. The Brunauer–Emmett–Teller (BET) equation was used for surface area analysis, and the Barrett–Joyner–Halenda (BJH) model was used for pore volume analysis.

Metal loading (%) was studied using a Perkin-Elmer Optima 4300 ICP-OES to measure the Cu content present in the catalysts.

H_2 temperature-programmed reduction (H_2-TPR) analysis was carried out using a Micromeritics AutoChem II instrument to analyse the reducibility of the catalysts. Samples (0.1 g) were loaded inside a quartz U-tube and heated to 800 °C from room temperature at a rate of 15 °C min^{-1} under 10% H_2–Ar.

Transmission electron microscopy (TEM) was carried out using a Thermo Fisher Talos F200X G2 operated at 200 kV. Samples were prepared for TEM by mixing the catalyst in

842 | Catal. Sci. Technol., 2024, 14, 840–849

This journal is © The Royal Society of Chemistry 2024

ethanol and sonicating it for 5 min to avoid any agglomeration. The sample was then drop-casted on the TEM grid.

2.4 Catalytic activity

Hydrogenation reaction of LA to GVL was carried out using a 100 ml Autoclave Engineers' reactor having pressure and temperature limits of 200 bar and 200 °C respectively. For catalyst activity testing, prior to the hydrogenation reaction, catalyst pre-reduction was performed at 200 °C at 20 bar H_2 pressure for 2 h. The reactor was charged with 200 mg of the catalyst and 30 ml of 1,4-dioxane : water (3 : 7 mol ratio) for catalyst pre-reduction and purged with H_2 to remove any residual gas. The reactor was then heated to 200 °C, to pressurized with 20 bar H_2 and stirred at 1500 rpm for 2 h. After pre-reducing the catalyst, the reactor was cooled and then 1 g LA was charged in the reactor and purged four times with H_2. Thereafter the reactor was heated to 190 °C and to pressurized with 20 bar H_2 and agitated to 1500 rpm; this was measured to be time zero. In our previous study, using design of experiment (DoE) to optimisation, we found 190 °C temperature, 20 bar H_2 pressure, and speed of agitation at 1500 rpm as the optimum reaction conditions for LA hydrogenation.[31] During the reaction, small aliquots of the sample were collected, filtered, and analysed using a Perkin-Elmer Clarus 500 GC fitted with a Zebron ZB-Wax column (30 m, 0.32 mm, and 0.25 mm) and an FID detector. Tetrahydrofuran (THF) was used an internal standard.

Turnover frequency, TOF (h^{-1}) was calculated based on low conversions obtained at 1 h, using the following equation:

$$\text{Turnover frequency, TOF} = \frac{\text{moles of LA converted}}{\text{moles of Cu} \times h}$$

3. Results and discussion

3.1 Catalyst to characterisation

A series of Cu/OMS-2 catalysts with 5, 10 and 20 wt% Cu loading was prepared using Wet-Imp and Pre-Dep methods. The synthesized materials were thoroughly to characterised,

and the structural properties such as measured Cu content, BET specific surface area and pore volume are given in Table 1. The comparison of theoretical and measured Cu wt% using ICP analysis is also shown, which indicated that similar Cu wt% loadings were achieved using different catalyst preparation methods. From structural properties, at first, it is noticed that there is a distinct and measurable effect of the catalyst preparation method on the structural properties. For instance, the BET surface areas were noticeably higher when catalysts with similar Cu wt% loadings were prepared using the Pre-Dep method as compared to the Wet-Imp method. A similar trend for an increase in the pore volume is also noticed, 0.107–0.145 cm^3 g^{-1} in Wet-Imp catalysts, which increased to 0.184–0.187 cm^3 g^{-1} in Pre-Dep catalysts (Table 1). The above trends could be attributed to the difference in the Cu NP sizes, and Cu metal dispersion on the surface. Both set of catalysts were analysed using X-ray diffraction analysis, and the corresponding XRD patterns are shown in Fig. 1. The peaks at 2θ values of 28.7°, 37.5, 41.9°, 50.0°, 60.1 and 65.2° correspond to the cryptomelane structure of manganese oxide OMS-2 material.[51,52] Fig. 1(a) shows Cu peaks at 43.3° (111) and 74.13° (220).[53] The CuO phase appears as a sharp peak at 38.9° (200) which confirms that CuO is monoclinic and is consistent with the peaks of the CuO standard PDF #48-1548. Diffraction peaks of cuprite were also observed at angles 32.6° (110) and 36.2° (111) respectively.[54]

For Wet-Imp 5, 10 and 20 wt% Cu/OMS-2 catalysts, the average Cu crystallite sizes were calculated using the Scherer equation, and found to be 19.8, 20.9 and 22.9 nm respectively. Similarly, the Cu crystallite average size from Pre-Dep catalysts was calculated from Fig. 1(b) diffraction peaks of 36.2° and 38.8°. The average size from XRD data was calculated to be 11.2 and 14.1 nm for 10, and 20 wt% Cu/OMS-2 catalysts. No peaks corresponding to Cu were seen in the XRD patterns for the Prep-Dep 5 wt% Cu/OMS-2 catalyst, which indicated smaller Cu crystallites with high dispersion of Cu metal on the support.

To further investigate the smaller Cu crystallites, 5 wt% Cu/OMS-2 prepared by both Pre-Dep and Wet-Imp methods were investigated using TEM analysis. Fig. 2(a) corresponds to the 5 wt% Cu/OMS-2 (Pre-Dep) catalyst, and shows well

Table 1 Physical properties of Cu/OMS-2 catalysts

Catalysts		Measured Cu[a] (wt%)	Specific surface area[b] (m^2 g^{-1})	Pore volume[c] (cm^3 g^{-1})	Average Cu crystallite size (nm)	
					XRD analysis[d]	TEM analysis[e]
Wet-Imp Cu/OMS-2	5 wt%	5.06	27.3	0.145	19.8	19.2
	10 wt%	10.80	23.6	0.113	20.9	20.0
	20 wt%	20.91	20.7	0.107	22.9	22.0
Pre-Dep Cu/OMS-2	5 wt%	5.37	68.9	0.187	—	2.6
	10 wt%	10.90	58.8	0.164	11.2	11.9
	20 wt%	20.32	42.2	0.184	14.1	14.6
OMS-2		—	76.1	0.250	—	—

[a] Measured using ICP-OES. [b] Measured using BET analysis. [c] Determined using the BJH method. [d] Calculated using Scherrer's eqn. [e] Measured using ImageJ software.

This journal is © The Royal Society of Chemistry 2024

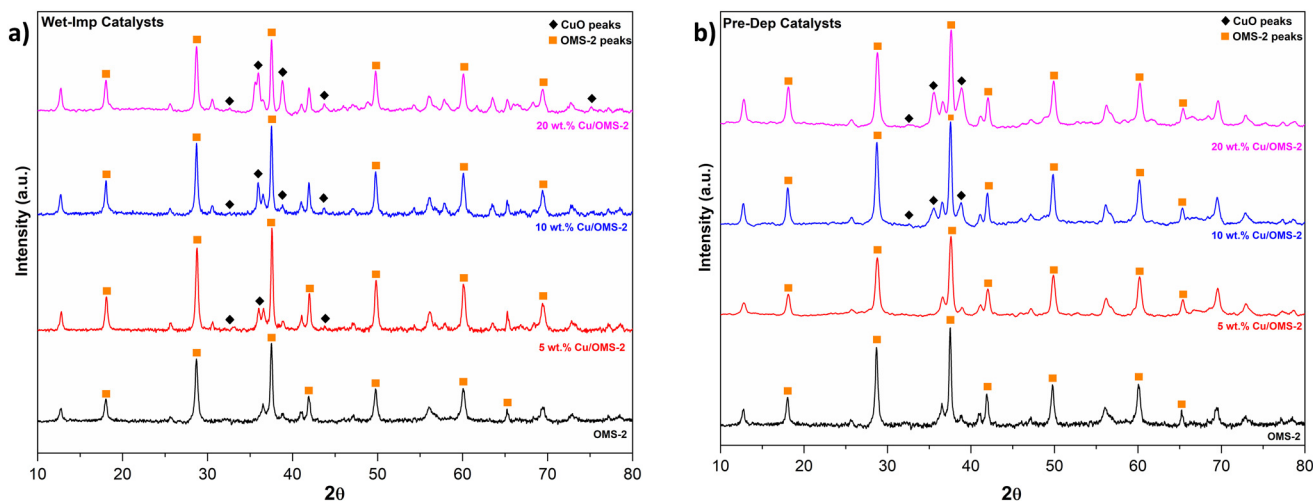*Catal. Sci. Technol.*, 2024, **14**, 840–849 | **843**

Fig. 1 XRD patterns of Cu/OMS-2 catalysts prepared by the (a) Wet-Imp; (b) Pre-Dep method.

defined manganese oxide nanorods, doped with fine and uniformly dispersed small CuO nanoparticles. Fig. 2(b and c) exhibit the elemental mapping of Mn and Cu, which further confirms the even distribution and small size of the CuO nanoparticles. Fig. 2(d) shows the histogram with narrow particle size distribution, with an average CuO particle size of 2.6 nm. This finding correlates with Fig. 1(b), where no Cu diffraction peaks were seen in the XRD patterns, indicating that the Cu particles were highly dispersed and small, making it not visible in the XRD patterns. In Fig. 2(e), a

brightfield TEM image of 5 wt% Cu/OMS-2 (Wet-Imp) catalyst demonstrates a clear view of a CuO particle located noticeably on top of a manganese oxide OMS-2 nanorod. This particle is remarkably larger when compared to the Pre-Dep catalyst. Fig. 2(f and g), shows the HAADF-STEM image of the catalyst, clearly demonstrating that large CuO agglomerates have formed over the support and overlaid elemental mapping reveals that the particles are not as well-dispersed compared to the Pre-Dep catalyst shown in Fig. 2(c). The size distribution histogram in Fig. 2(h) implies an average CuO
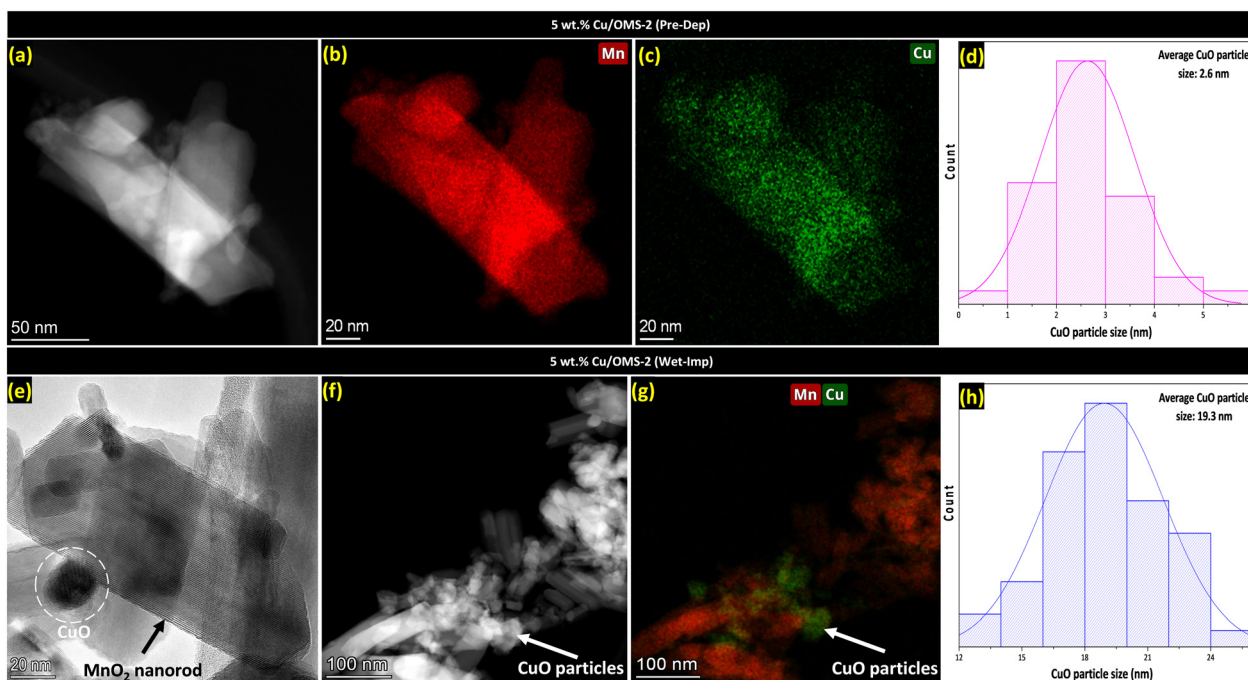

Fig. 2 TEM analysis for 5 wt% Cu/OMS-2 Pre-Dep (a)–(d), and 5 wt% Cu/OMS-2 Wet-Imp (e)–(h). (a) HAADF-STEM representative overview, EDX elemental maps for Mn (b), and (c) Cu, and (d) average particle size distribution of CuO nanoparticles. (e) Brightfield TEM image displaying a CuO nanoparticle in the white dotted circle, (f) HAADF-STEM representative overview, (g) EDX overlaid elemental maps of Mn and Cu, and (h) average particle size distribution of CuO nanoparticles.
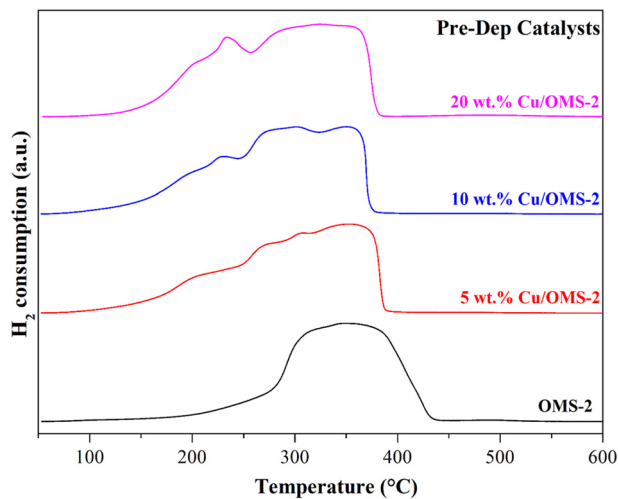
844 | *Catal. Sci. Technol.*, 2024, **14**, 840–849

This journal is © The Royal Society of Chemistry 2024

Fig. 3 H$_2$-TPR profiles of 5, 10 and 20 wt% Cu/OMS-2 catalysts prepared by the Pre-Dep method.

particle size of 19.3 nm, further supporting the non-uniform and heterogeneous deposition of CuO on the support.

To investigate the Cu reducibility, H$_2$-TPR analysis was performed. Fig. 3 shows the reduction profiles for pristine OMS-2, and 5, 10 and 20 wt% Cu/OMS-2 catalysts prepared using the Pre-Dep method. Cu supported on mixed metal oxides usually show different reduction patterns due to the surface interactions between copper oxide and support metal oxides. The bulk copper oxide reduces around 280 °C. In our materials, we observe the reduction peak at lower temperatures of around 200 °C, which can be attributed to smaller Cu nanoparticles.[55] The shoulder peak seen at a higher temperature can be attributed to Cu having strong metal–support interaction with manganese oxide.[56] The peak observed between 369 °C to 390 °C signifies the reduction of manganese oxide from Mn^{4+} to Mn^{3+} state.[34] Further, a comparison of the catalysts prepared by both methods, 20
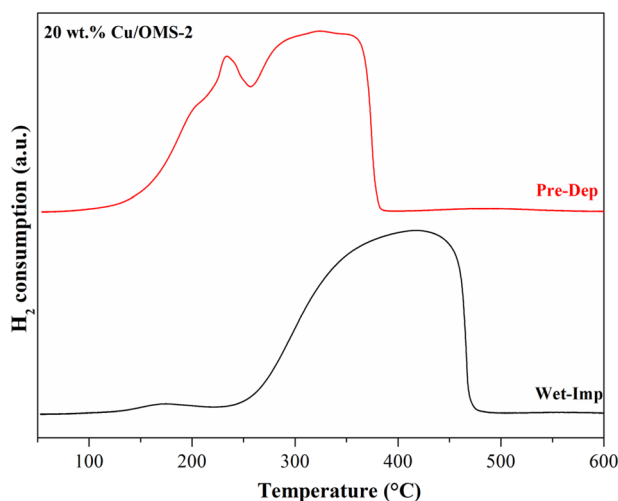
wt% Cu/OMS-2 (Pre-Dep *vs.* Wet-Imp) displayed significantly different reduction profiles (Fig. 4). The 20 wt% Cu/OMS-2 Prep-Dep catalyst showed a noticeably higher H$_2$ uptake as compared to the Wet-Imp catalyst, which could be due to the smaller CuO particle size with higher dispersion on the manganese oxide support.

3.2 Catalyst performance in LA hydrogenation

Both Wet-Imp and Pre-Dep catalysts were investigated under same reaction conditions for liquid phase hydrogenation of LA to GVL. The performance of each catalyst was evaluated under identical reaction conditions, in 30 ml of 1,4-dioxane and water (3 : 7 mol ratio) as solvent at 190 °C, 20 bar H$_2$, 1 g LA and 0.2 g of catalyst for 240 min. All catalysts prepared using the Prep-Dep method showed higher GVL yields as compared to the corresponding Wet-Imp catalysts. The GVL yield–time profiles are shown in Fig. 5(a–c). As shown in Fig. 5(a), the GVL yield (%) increased from 20 wt% Cu/OMS-2 Wet-Imp to Pre-Dep prepared catalysts. The same trend is also seen with 10 wt% Cu/OMS-2 (Fig. 5b) and 5 wt% Cu/OMS-2 (Fig. 5c) respectively. Full conversion of LA was reached within 4 h with all the Pre-Dep catalysts. The higher LA conversions and GVL yields, using Prep-Dep catalysts in comparison to the Wet-Imp catalysts for similar Cu wt% loadings, can be attributed to the relatively smaller CuO particle sizes, and overall higher specific surface area (Table 1).

Fig. 5(d and e) shows the X-ray diffraction (XRD) patterns of the pre-reduced Cu/OMS-2 catalysts prepared by Wet-Imp and Pre-Dep methods. The diffraction peaks observed at 2θ values 29.9°, 37.0°, 42.6° and 62.4° corresponds to the (110), (111), (200) and (220) crystal planes of the Cu$_2$O (Cu$^+$, cuprous oxide) phase with the space group $Pn\bar{3}m$ in accordance with the JCPDS no. 034-1354.[57] Peaks observed at 2θ values 43.6°, 50.7° and 74.4° are assigned to the (111), (200), and (220) planes of metallic copper (Cu^0), which are consistent with JCPDS no. 04-0836.[58] The XRD analysis of the pre-reduced catalysts infers that Cu NPs are in mixed crystalline phases of Cu$^+$ and Cu^0. It is plausible that both copper species Cu$^+$ and Cu^0 could contribute to improved catalytic performance, by participating in the reaction mechanism. Cu$^+$ acts as a Lewis acid site, interacting with the oxygen of the carbonyl group of LA, for formation of α-AL through dehydration,[59,60] and subsequently, Cu^0 facilitates the dissociation of hydrogen for the reduction of α-AL to GVL. The crystallite size of the pre-reduced catalysts prepared *via* Wet-Imp and Pre-Dep methods was determined using the Scherrer's equation for Cu^0 peaks. Three peaks (2θ values of 43.6°, 50.7° and 74.4°) were used separately to calculate the crystallite size and the average value was considered. For Wet-Imp catalysts, fresh 20 wt% Cu/OMS-2 was calculated to be 22.9 nm, while the pre-reduced catalyst measured slightly larger at 23.8 nm. Similarly, pre-reduced 10 and 5 wt% Cu/OMS-2 (Wet-Imp) were measured to be 21.4 nm and 21.0 nm, which are relatively close to the fresh catalysts (Table 1). A

Fig. 4 H$_2$-TPR profiles of 20 wt% Cu/OMS-2 catalysts prepared by Pre-Dep and Wet-Imp methods.

This journal is © The Royal Society of Chemistry 2024

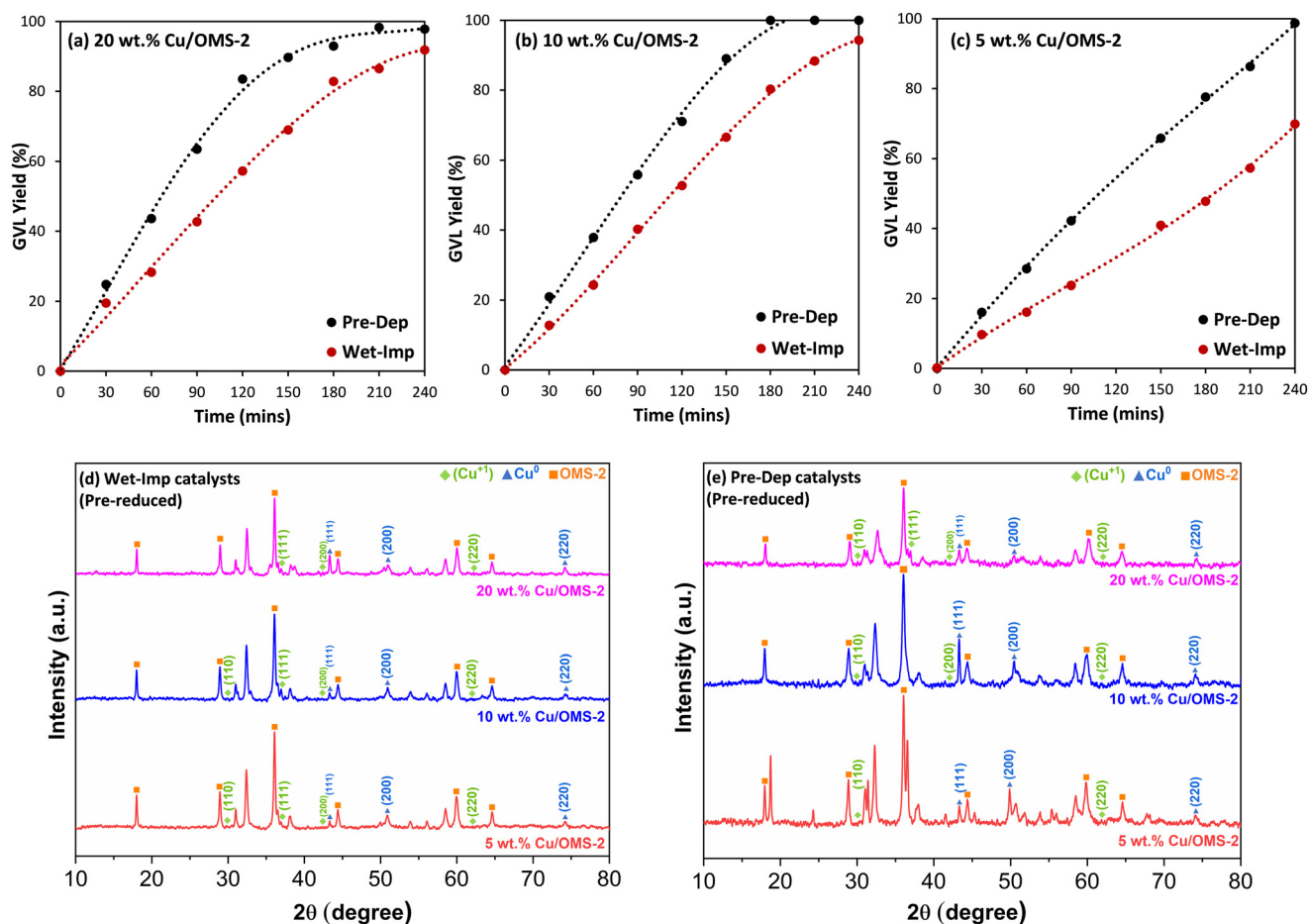*Catal. Sci. Technol.,* 2024, **14**, 840–849 | **845**

Fig. 5   GVL yield (%) in LA hydrogenation using (a) 20 wt% Cu/OMS-2; (b) 10 wt% Cu/OMS-2 and (c) 5 wt% Cu/OMS-2. Reaction conditions: 1 g LA, 30 ml solvent (1,4-dioxane and water in 3 : 7 mol ratio), 0.2 g of catalyst at 190 °C temperature and 20 bar H_2 pressure for 240 min at 1500 rpm; XRD patterns of pre-reduced 5, 10 and 20 wt% Cu/OMS-2 catalysts prepared by (d) Wet-Imp, and (e) Pre-Dep methods.

similar trend can be observed in the Pre-Dep catalysts, with the crystallite size measuring to be 15.8 nm (20 wt% Cu/OMS-2), 13.2 nm (10 wt% Cu/OMS-2) and 4.7 nm (5 wt% Cu/OMS-2). The crystallite size closely corresponds to that of the
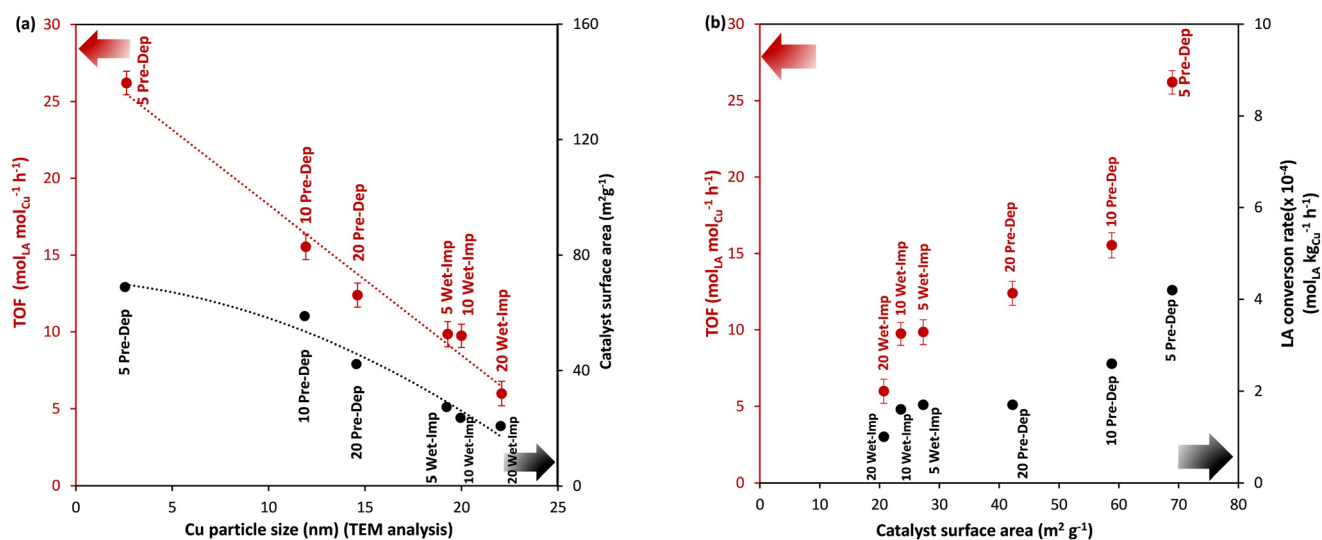

Fig. 6   (a) TOF; and (b) LA conversion rate as a function of catalyst surface area for Cu/OMS-2.

Catalysis Science & Technology

fresh catalysts, indicating that both the fresh and pre-reduced catalysts exhibit the same Cu size.

3.3 Effect of Cu nanoparticle size on the catalytic activity

The effect of Cu size on the catalytic activity in the hydrogenation of LA to GVL was studied by comparing the TOF (h^{-1}) values and catalyst surface area ($m^2 \ g^{-1}$) (Fig. 6a) as a function of the Cu nanoparticle sizes as determined by TEM. The TOF values are a good activity performance indicator. Amongst the catalysts evaluated in our study, the maximum TOF value of 27 h^{-1} was achieved using the 5 wt% Cu/OMS-2 catalyst (Cu NP size 2.6 nm). Meanwhile, in comparison, the TOF values of 16.2 h^{-1} for 10 wt% Cu/OMS-2, and 10.5 h^{-1} for 20 wt% Cu/OMS-2 catalysts were achieved. Thus, TOF values show a linear dependency on the Cu NP sizes, and TOF values increase as the Cu NP size decrease (Fig. 6a). A similar dependency is also observed for the catalyst surface area of the catalysts and size of the Cu nanoparticles; surface areas increase as the Cu NP size decrease (Fig. 6a). As a rule, a horizontal line in the plot of TOF *vs.* metal nanoparticle size or surface area is indicative of a structure-insensitive reaction. Therefore, LA hydrogenation to GVL is a structurally sensitive reaction as the TOF ($mol_{LA} \ mol_{Cu}^{-1} \ h^{-1}$) indicated dependency on theCu nanoparticle size. Similarly, in the Wet-Imp catalysts, as the Cu wt% increased, the Cu NP size increased, and the corresponding TOF values decreased, with the lowest TOF of 6.2 h^{-1} from 20 wt% Cu/OMS-2 with the Cu particle size of 22 nm. The best performing catalyst, the 5 wt% Cu/OMS-2 Pre-Dep catalyst (TOF 27 h^{-1}), has the highest catalyst surface area of 68.9 $m^2 \ g^{-1}$ and demonstrated the maximum LA conversion rate of $4.2 \times 10^{-4} \ mol_{LA} \ kg_{Cu}^{-1} \ h^{-1}$. Fig. 6b shows a proportional increase in LA conversion rate ($mol_{LA} \ kg_{Cu}^{-1} \ h^{-1}$) as the surface area of the Cu catalysts increased. A similar linear correlation of catalytic activity and surface area in catalysts which are supported on various metal oxides have been reported by other research groups.[50,61] For instance, Kon *et al.* using the Pt/HMFI zeolite catalyst observed a TOF of 33 h^{-1}.[62] Zhang *et al.* have reported TOF values of 278 h^{-1} using single atom catalyst Ru on TiO$_2$@nitrogen doped carbon support, and 7.9 h^{-1} using commercial Ru/C as the catalyst.[63] In their study, high TOF values were attributed to single atom catalysis and the use of N$_2$ in the reaction feed. In a separate study, Liu *et al.* using Ni and NiO supported on mesoporous carbon, observed the TOF of 10.8 h^{-1} in LA hydrogenation.[64] In our studies, we obtained the TOF values of 27 h^{-1} for 5 wt% Cu/OMS-2 (Pre-Dep) and 10.6 h^{-1} for 5 wt% Cu/OMS-2 (Wet-Imp).

It has been reported that ratio of (111) and (100) facets, corner or edge atoms are influenced by particle size, which in turn influences the structural and electronic properties of the catalyst and larger particles are exposed to fewer edges, defects and low-index facets in comparison to smaller crystallite sizes.[65] Smaller sized crystallites have more open planes, edges and defects, which comprises of co-ordinated unsaturated species which are more reactive in contrast to fully coordinated species. As the size of Cu nanoparticles decrease, the interaction with metal oxide support increases, which might involve the role of support in activity as well. The trend seen from the range of catalysts prepared with different methods clearly indicate that the activity trend correlates well with Cu particle size, thereby indicating it as the primary factor for activity.

4. Conclusions

We have shown the performance of Cu/OMS-2 catalysts prepared by different methods, wet impregnation and precipitation deposition, in the hydrogenation of LA to GVL using 1,4-dioxane and water as solvents. Best results were obtained using the 20, 10 and 5 wt% Cu/OMS-2 precipitation deposition catalysts which showed an increased LA conversion and GVL yield as compared to wet impregnation catalysts. Considering the TOF value as a descriptor for the performance of catalysts, we found that the 5 wt% Cu/OMS-2 Pre-Dep catalyst to be the best, which had a TOF value of 27 $mol_{LA} \ mol_{Cu}^{-1} \ h^{-1}$. Catalyst characterisation established the difference of preparation methods which leads to different Cu particle sizes. It was shown that LA hydrogenation in 1,4-dioxane and water is structure sensitive. Based on our data, with Cu nanoparticle sizes prepared in the range of 2 to 22 nm, the Cu NP size of 2 nm was accomplished using the precipitation deposition method.

Author contributions

N. J. M.: methodology, investigation and writing – original draft preparation. P. K. and M. A.: TEM measurements, analysis and draft preparation. N. A.: methodology and draft revision. H. M.: conceptualisation, visualisation, validation, writing – review & editing and resources.

Conflicts of interest

There are no conflicts to declare.

Acknowledgements

Notes and references

1 W. R. H. Wright and R. Palkovits, *ChemSusChem*, 2012, **5**, 1657–1667.

2 M. Sudhakar, V. V. Kumar, G. Naresh, M. L. Kantam, S. K. Bhargava and A. Venugopal, *Appl. Catal., B*, 2016, **180**, 113–120.

3 J. K. Nørskov, T. Bligaard, B. Hvolbæk, F. Abild-Pedersen, I. Chorkendorff and C. H. Christensen, *Chem. Soc. Rev.*, 2008, **37**, 2163.

4 A. S. Crampton, M. D. Rötzer, C. J. Ridge, B. Yoon, F. F. Schweinberger, U. Landman and U. Heiz, *Surf. Sci.*, 2016, **652**, 7–19.

5 B. Roldan Cuenya and F. Behafarid, *Surf. Sci. Rep.*, 2015, **70**, 135–187.

6 R. A. Van Santen, *Acc. Chem. Res.*, 2009, **42**, 57–66.

7 R. Van Den Berg, G. Prieto, G. Korpershoek, L. I. Van Der Wal, A. J. Van Bunningen, S. Lægsgaard-Jørgensen, P. E. De Jongh and K. P. De Jong, *Nat. Commun.*, 2016, **7**, 13057.

8 Z. P. Liu and P. Hu, *J. Am. Chem. Soc.*, 2003, **125**, 1958–1967.

9 F. Calle-Vallejo, D. Loffreda, M. T. M. Koper and P. Sautet, *Nat. Chem.*, 2015, **7**, 403–410.

10 L. Castoldi, R. Matarrese, L. Kubiak, M. Daturi, N. Artioli, S. Pompa and L. Lietti, *Catal. Today*, 2019, **320**, 141–151.

11 J. Wisniewska, M. Ziolek, N. Artioli and M. Daturi, *J. Catal.*, 2016, **336**, 58–74.

12 L. Lietti, N. Artioli, L. Righini, L. Castoldi and P. Forzatti, *Ind. Eng. Chem. Res.*, 2012, **51**, 7597–7605.

13 J. Tan, J. Cui, T. Deng, X. Cui, G. Ding, Y. Zhu and Y. Li, *ChemCatChem*, 2015, **7**, 508–512.

14 C. Ortiz-Cervantes and J. J. García, *Inorg. Chim. Acta*, 2013, **397**, 124–128.

15 W. Luo, U. Deka, A. M. Beale, E. R. H. Van Eck, P. C. A. Bruijnincx and B. M. Weckhuysen, *J. Catal.*, 2013, **301**, 175–186.

16 IEA, *World Energy Investment 2023*, IEA, Paris, 2023.

17 IEA, *CO2 Emissions in 2022*, IEA, Paris, 2023.

18 J. Salisu, N. Gao, C. Quan, J. Yanik and N. Artioli, *J. Energy Inst.*, 2023, **108**, 101239.

19 S. Kang, J. Fu and G. Zhang, *Renewable Sustainable Energy Rev.*, 2018, **94**, 340–362.

20 Z. Yu, X. Lu, J. Xiong and N. Ji, *ChemSusChem*, 2019, **12**, 3915–3930.

21 S. Dutta, I. K. M. Yu, D. C. W. Tsang, Y. H. Ng, Y. S. Ok, J. Sherwood and J. H. Clark, *Chem. Eng. J.*, 2019, **372**, 992–1006.

22 M. A. Díaz-Pérez and J. C. Serrano-Ruiz, *Molecules*, 2020, **25**, 802.

23 J. Q. Bond, D. M. Alonso, D. Wang, R. M. West and J. A. Dumesic, *Science*, 2010, **327**, 1110–1114.

24 A. M. Hengne and C. V. Rode, *Green Chem.*, 2012, **14**, 1064.

25 L. Zhang, J. Mao, S. Li, J. Yin, X. Sun, X. Guo, C. Song and J. Zhou, *Appl. Catal., B*, 2018, **232**, 1–10.

26 I. Orlowski, M. Douthwaite, S. Iqbal, J. S. Hayward, T. E. Davies, J. K. Bartley, P. J. Miedziak, J. Hirayama, D. J. Morgan, D. J. Willock and G. J. Hutchings, *J. Energy Chem.*, 2019, **36**, 15–24.

27 S. Pendem, I. Mondal, A. Shrotri, B. S. Rao, N. Lingaiah and J. Mondal, *Sustainable Energy Fuels*, 2018, **2**, 1516–1529.

28 Q. Xu, X. Li, T. Pan, C. Yu, J. Deng, Q. Guo and Y. Fu, *Green Chem.*, 2016, **18**, 1287–1294.

29 A. Karelovic and P. Ruiz, *Catal. Sci. Technol.*, 2015, **5**, 869–881.

30 Z. Li, Z. Hao, J. Lu, C. Wu, R. Gao, J. Li, C.-L. Liu and W.-S. Dong, *J. Energy Chem.*, 2021, **61**, 446–458.

31 N. J. Mazumdar, G. Deshmukh, A. Rovea, P. Kumar, M. Arredondo-Arechavala and H. Manyar, *R. Soc. Open Sci.*, 2022, **9**, 220078.

32 W. Gong, C. Chen, R. Fan, H. Zhang, G. Wang and H. Zhao, *Fuel*, 2018, **231**, 165–171.

33 A. M. Ruppert, J. Grams, M. Jędrzejczyk, J. Matras-Michalska, N. Keller, K. Ostojska and P. Sautet, *ChemSusChem*, 2015, **8**, 1538–1547.

34 I. J. McManus, H. Daly, H. G. Manyar, S. F. R. Taylor, J. M. Thompson and C. Hardacre, *Faraday Discuss.*, 2016, **188**, 451–466.

35 C. Coney, C. Hardacre, K. Morgan, N. Artioli, A. P. E. York, P. Millington, A. Kolpin and A. Goguet, *Appl. Catal., B*, 2019, **258**, 117918.

36 G. D. Yadav and H. G. Manyar, *Adv. Synth. Catal.*, 2008, **350**, 2286–2294.

37 C. Quan, G. Zhang, N. Gao, S. Su, N. Artioli and D. Feng, *Energy Fuels*, 2022, **36**, 8311–8322.

38 J. Ethiraj, D. Wagh and H. Manyar, *Energy Fuels*, 2022, **36**, 1189–1204.

39 K. Pandit, C. Jeffrey, J. Keogh, M. S. Tiwari, N. Artioli and H. G. Manyar, *Ind. Eng. Chem. Res.*, 2023, **62**, 9201–9210.

40 T. Jakubek, K. Ralphs, A. Kotarba and H. Manyar, *Catal. Lett.*, 2019, **149**, 100–106.

41 T. Jakubek, C. Hudy, J. Gryboś, H. Manyar and A. Kotarba, *Catal. Lett.*, 2019, **149**, 2218–2225.

42 R. O'Donnell, K. Ralphs, M. Grolleau, H. Manyar and N. Artioli, *Top. Catal.*, 2020, **63**, 351–362.

43 M. T. Yilleng, E. C. Gimba, G. I. Ndukwe, I. M. Bugaje, D. W. Rooney and H. G. Manyar, *J. Environ. Chem. Eng.*, 2018, **6**, 6382–6389.

44 T. G. A. Youngs, H. Manyar, D. T. Bowron, L. F. Gladden and C. Hardacre, *Chem. Sci.*, 2013, **4**, 3484.

45 K. Ralphs, G. Collins, H. Manyar, S. L. James and C. Hardacre, *ACS Sustainable Chem. Eng.*, 2022, **10**, 6934–6941.

46 M. T. Rahman, S. Wharry, M. Smyth, H. Manyar and T. S. Moody, *Synlett*, 2020, **31**, 581–586.

47 H. G. Manyar, R. Morgan, K. Morgan, B. Yang, P. Hu, J. Szlachetko, J. Sá and C. Hardacre, *Catal. Sci. Technol.*, 2013, **3**, 1497.

48 X. Chen, Z. Wang, H. Daly, R. Morgan, H. Manyar, C. Byrne, A. S. Walton, S. F. R. Taylor, M. Smith, R. Burch, P. Hu and C. Hardacre, *Appl. Catal., A*, 2020, **593**, 117420.

49 H. G. Manyar, B. Yang, H. Daly, H. Moor, S. McMonagle, Y. Tao, G. D. Yadav, A. Goguet, P. Hu and C. Hardacre, *ChemCatChem*, 2013, **5**, 506–512.

50 S. Natesakhawat, J. W. Lekse, J. P. Baltrus, P. R. Ohodnicki, B. H. Howard, X. Deng and C. Matranga, *ACS Catal.*, 2012, **2**, 1667–1676.

51 S. Sithambaram, E. K. Nyutu and S. L. Suib, *Appl. Catal., A*, 2008, **348**, 214–220.

848 | *Catal. Sci. Technol.*, 2024, **14**, 840–849

This journal is © The Royal Society of Chemistry 2024

52 K. Wantala, T. Suwannaruang, J. Palalerd, P. Chirawatkul, N. Chanlek, S. Wannapaiboon, C. Saiyasombat and R. Khunphonoi, *Surf. Interfaces*, 2021, **23**, 101030.

53 D. Mardiansyah, T. Badloe, K. Triyana, M. Q. Mehmood, N. Raeis-Hosseini, Y. Lee, H. Sabarman, K. Kim and J. Rho, *Sci. Rep.*, 2018, **8**, 10639.

54 D. Zhu, L. Wang, W. Yu and H. Xie, *Sci. Rep.*, 2018, **8**, 5282.

55 J. Y. Kim, J. A. Rodriguez, J. C. Hanson, A. I. Frenkel and P. L. Lee, *J. Am. Chem. Soc.*, 2003, **125**, 10684–10692.

56 J. Zhang, X. Meng, C. Yu, G. Chen and P. Zhao, *RSC Adv.*, 2015, **5**, 87221–87227.

57 C. Tang, X. Ning, J. Li, H.-L. Guo and Y. Yang, *J. Mater. Sci. Technol.*, 2019, **35**, 1570–1577.

58 M. Salavati-Niasari, F. Davar and N. Mir, *Polyhedron*, 2008, **27**, 3514–3518.

59 S. Zhu, X. Gao, Y. Zhu, Y. Zhu, H. Zheng and Y. Li, *J. Catal.*, 2013, **303**, 70–79.

60 S. Zhu, X. Gao, Y. Zhu, W. Fan, J. Wang and Y. Li, *Catal. Sci. Technol.*, 2015, **5**, 1169–1180.

61 C. Baltes, S. Vukojevic and F. Schuth, *J. Catal.*, 2008, **258**, 334–344.

62 K. Kon, W. Onodera and K. Shimizu, *Catal. Sci. Technol.*, 2014, **4**, 3227–3234.

63 K. Zhang, Q. Meng, H. Wu, T. Yuan, S. Han, J. Zhai, B. Zheng, C. Xu, W. Wu, M. He and B. Han, *Green Chem.*, 2021, **23**, 1621–1627.

64 X. Liu and Z. Li, *Sustainable Energy Fuels*, 2021, **5**, 3312–3320.

65 D. Uzio and G. Berhault, *Catal. Rev.: Sci. Eng.*, 2010, **52**, 106–131.

This journal is © The Royal Society of Chemistry 2024

Catal. Sci. Technol., 2024, **14**, 840–849 | **849**